Assessing the accuracy of TD-DFT excited-state geometries through optimal tuning with GW energy levels

Iryna Knysh, Denez Raimbault, Ivan Duchemin, Xavier Blase, Denis Jacquemin

Assessing the accuracy of TD-DFT excited-state geometries through optimal tuning with *GW* energy levels

Iryna Knysh,[1] Denez Raimbault,[1] Ivan Duchemin,[2] Xavier Blase,[3] and Denis Jacquemin[1,4]
[1)]*Nantes Université, CNRS, CEISAM UMR 6230, F-44000 Nantes, France*
[2)]*Université Grenoble Alpes, CEA, IRIG-MEM-L_Sim, 38054 Grenoble, France*
[3)]*Université Grenoble Alpes, CNRS, Institut Néel, F-38042 Grenoble*
[4)]*Institut Universitaire de France, 75005 Paris, France*

(*Electronic mail: Denis.Jacquemin@univ-nantes.fr)

(*Electronic mail: xavier.blase@neel.cnrs.fr)

We study the accuracy of excited state (ES) geometries using optimally tuned LC-PBE functionals with a tuning based on *GW* quasiparticle energies. We compare the results obtained with the PBE, PBE0, non-tuned and tuned LC-PBE functionals with available high-level CC reference values as well as experimental data. First, we compare ES geometrical parameters obtained for three different types of systems: molecules composed of a few atoms, 4-(dimethylamino)benzonitrile (DMABN), and conjugated dyes. To this end, we used wave-function results as benchmarks. Next, we evaluate the accuracy of the theoretically simulated spectra as compared to experimental ones for five large dyes. Our results show that besides small compact molecules, for which tuning LC-PBE does not allow obtaining geometries more accurate than those computed with standard functionals, tuned range-separated functionals are clearly to be favored, not only for ES geometries, but also for 0-0 energies, band shapes and intensities for absorption and emission spectra. Particularly, the results indicate that *GW*-tuned LC-PBE functionals provide an improved matching with experimental spectra as compared to the conventionally tuned functional. It is an open question whether TD-DFT with *GW*-tuned functionals can qualitatively mimic the actual many-body Bethe-Salpeter (BSE/*GW*) formalism for which analytic ionic gradients remain to be developed.

I. INTRODUCTION

The interaction of organic molecules with light leads to a variety of fascinating excited-state (ES) processes such as fluorescence and phosphorescence, photoswitching, thermally activated delayed fluorescence (TADF), *etc.* During the last few decades, numerous applications based on these phenomena were developed, *e.g.*, organic light-emitting diodes (OLED), fluorescent sensors, and advanced bioimaging technologies.[1–4] To optimize the efficiency of these applications, it is necessary to adapt the structure of the active molecule so as to fine-tune its excited-state properties. In particular, for the emission properties, an analysis of the ES potential energy surfaces (PES), and more specifically of the key geometries on these PES, can hint at possible non-radiative deactivation mechanisms, and consequently loss of device efficiency. However, access to ES structures remains limited. Experimental determination of ES geometries is always complex and typically limited to molecules consisting of few atoms.[5–7] In this framework, theoretical methods have the edge since they allow obtaining different ES structures including ES minima, transition states (TS), conical intersections (CI), and minimum energy crossing points (MECP). There is a large panel of methods which can be used for geometry optimizations. Nevertheless, each method has its own limitations. High-level theories, *e.g.*, coupled-cluster (CC) and complete active space self-consistent field (CASSCF) methods, are known to provide accurate geometries but they can be applied only to compact systems. The studies of "real-life" dyes are usually performed using time-dependent density functional (TD-DFT) theory.[8–10] However, the quality of obtained ES geometries remains dependent on the choice of exchange-correlation functional (XCF).[11–14] For instance, generalized gradient approximations (GGA) and global hybrid XCF are known to provide qualitatively inaccurate PES for ES showing a strong charge-transfer (CT) character.[15–17] The origin of the TD-DFT failure for the excited states having CT character is the poor description of the nonlocal electron-hole interactions by standard DFT methods.[15,16] Using range-separated hybrid functionals (RSH), that present a growing fraction of *exact* exchange with increasing interelectron distance, can lead to a more accurate description of these interactions.[18,19] Popular RSH, *e.g.*, CAM-B3LYP[20] or ωB97X-D,[21] have a range-separated parameter ω, that controls the exact/DFT exchange admixture, defined by parametrization, meaning that ω was fitted to minimize target properties on a test set of molecules.[22] Another way to determine ω, known as optimal tuning (OT),[23] aims to comply with the DFT ionization potential theorem for any single molecule, so that ω becomes system dependent. In OT-RSH functionals ω values are typically obtained as the one that satisfies[23,24]

$$\mathrm{IP}(N) = -\varepsilon_{\mathrm{HOMO}}(N), \tag{1}$$

where the ionization potential (IP) is calculated as a difference between the total energies of the neutral (N) and cationic ($N-1$) systems with N the number of electrons. We note that other approaches can be used.[25] Even though this OT scheme is more computationally expensive, since one needs to determine the ω for each molecule, it delivers improvements over non-tuned TD-DFT functionals for various ground-state (GS) and ES properties.[26–32] We note that Ju *et al.*[33] developed a machine learning model to determine ω, hence significantly reducing computational costs of such calculations.

An attractive alternative to TD-DFT is the many-body Green's function Bethe-Salpeter equation (BSE) formalism[34–40] relying on the *GW* self-energy and related

quasiparticle energies representing proper addition and removal energies.[41–44] Due to an accurate description of the screened electron-hole interactions, BSE/*GW* was shown to outperform TD-DFT for the calculation of the energies and properties of molecular systems, particularly those involving charge-transfer (CT) ES.[45–53] However, the main drawback of BSE/*GW* is the absence of an efficient analytical scheme for geometry optimizations, *e.g.*, contrary to TD-DFT no linear response techniques such as the *Z*-vector approach[54] is available yet for BSE/*GW* nuclear gradients. The Z-vector formalism combined with the BSE/*GW* formalism has been proposed recently, but only for excited states dipoles, namely electric fields gradients.[55] Nevertheless, a few studies treating ES optimizations with BSE/*GW* using alternative strategies can be found. In a seminal contribution, Ismail-Beigi and Louie proposed an analytic formalism, combined with approximations aiming at reducing its computational cost, for the calculation of ES forces with BSE/*GW*.[56] They showed that the BSE/*GW* formalism can correctly reproduce the variation of ES energies upon structural deformation of photoexcited carbon dioxide and ammonia. Later on, Kaczmarski and Rohlfing developed a diabatization scheme based on the so-called Baer method and applied it to the many-body BSE/GW formalism to study photoexcited compounds.[57] This BSE/*GW* diabatization method was used to describe the adiabatic and diabatic lowest excited electronic states of the retinal chromophore molecule.[58] This work showed that BSE/*GW* can be used to accurately predict the PES evolution of the ES during the photoisomerisation of retinal. Importantly, a benchmark study dealing with ES optimizations of four small molecules (carbon monoxide, acetone, acrolein, and methylenecyclopropene) performed using non-self-consistent BSE/G_0W_0 and eigenvalue-self-consistent BSE/ev*GW*[59,60] numerical gradients has been published recently.[61] In this contribution BSE/*GW* results were compared to CAS perturbation theory (CASPT2), variational Monte Carlo (VMC), second-order approximate CC (CC2), and TD-DFT data. This work concluded that the BSE/*GW* can provide ES geometries with an average relative error of *ca.* 1% for the BSE/G_0W_0 and 1.5% for BSE/ev*GW* schemes when taking CASPT2 results as references. Furthermore, our groups recently assessed the ability of BSE/ev*GW* to reproduce the ES PES along the twisting coordinate of 4-(dimethylamino)benzonitrile (DMABN) and N-phenylpyrrole (N-PP).[62,63] Our results showed that BSE/*GW* can produce accurate ES surfaces along this coordinate, especially in the cases that are challenging for TD-DFT, *i.e.*, for ES showing mixed local excited (LE) and CT characters.

In order to evaluate the accuracy of theoretically estimated ES geometries, one may use experimental absorption and emission spectra. Indeed, theoretical simulations of the optical spectra involve determining (or estimating) the PES of initial and final states. Consequently, one can indirectly evaluate the quality of the ES geometries obtained with different quantum chemistry methods by comparing the shapes of theoretical and experimental spectra.[64–66] Such experimental data are easily available for numerous compounds, even in the form of a database.[67] However, one needs to be cautious with the choice of the molecules: absorption and emission bands should be well resolved and rigid structures are more suitable for theoretical simulations; otherwise one needs to account for anharmonic effects, which dramatically increases the computational costs.[68,69] In addition, theoretical modelling of the vibronic spectra depends on several parameters: (i) the model to expand the ES PES, adiabatic (PES is built using ES energies, gradients, and Hessian computed at the GS and ES geometries)[66,70,71] or vertical (ES PES is expanded around the ES normal modes computed at starting equilibrium geometry),[66]; (ii) the dipole moment expansion, Franck-Condon (FC) or Herzberg-Teller (HT),[66,70,71] and (iii) the selected set of coordinates. As a consequence of all these possibilities, one does not only assess the quality of the electronic structure method to model the PES when comparing the experimental and theoretical spectra but also the vibronic approach itself.

In this work, we are exploring an alternative strategy to obtain accurate excited-state geometries by using an OT RSH functional tuned using the IP and electron affinities (EA) provided by the *GW* approach. This allows us to obtain a DFT functional mimicking the effect of the *GW* self-energy, yielding by derivation a TD-DFT kernel that may be possibly viewed as an approximation to its BSE analog. Optimally tuned functionals have been shown to yield good TD-DFT vertical excitation energies, including charge-transfer excitations.[72] Additionally, Kretz and Egger[73] showed that OT-RSH functional can also provide accurate geometries as well. Though OT RSH have been shown to be good starting point for subsequent *GW* calculations,[74] we propose here the reversed approach, using *GW* to perform OT. In that respect, the important benefit of this scheme is the availability of TD-DFT analytical gradients. We use these tuned functionals to explore the accuracy for geometry optimization, PES exploration, and vibronic spectra modelling. We divide the discussion of our results into two main parts: a comparison of the geometrical parameters (theory *vs* theory) and a modelling of the absorption and emission spectra (theory *vs* experiment). In the former, we use several systems: (i) a set of 10 small molecules for which high-level CC3[75] references are available; (ii) the challenging case of DMABN ES geometries for which we selected the Equation-of-Motion (EOM-)CCSD reference values[62]; and (iii) a set of 8 medium-sized conjugated systems with known CC2[76] reference values.[12] For the second part we select five quite rigid molecules from the PhotochemCAD™ database[67] with well-resolved spectra recorded in nonpolar solvents. Our main objective of this study is to assess the performance of LC-PBE functionals tuned on *GW* output compared to conventional OT procedure (as described above), and to compare it with the untuned LC-PBE functional,[19] other DFT functionals (PBE[77] and PBE0[77,78]), as well as CC methods (CC2 and CCSD).[79–82]

II. THEORY

A. Optimal-tuning of ω

The LC-PBE functional is an example of RSH functional where the Coulomb operator is split into two parts: the long-range (LR) and the short-range (SR) terms,[18]

$$\frac{1}{r_{12}} = \frac{1-\mathrm{erf}(\omega r_{12})}{r_{12}} + \frac{\mathrm{erf}(\omega r_{12})}{r_{12}}. \quad (2)$$

An important feature, in particular, is that the long-range non-local exchange contribution offers the proper tail in the vacuum, a desirable property shared with the *GW* self-energy. In Eq. (2), the range-separated parameter, ω, determines the evolution of the SR/LR ratio when the interelectronic distance, r_{12}, increases.[19,83] To obtain ω, the usual OT procedure proceeds by minimizng the $J^2(\omega)$ function,[72]

$$J^2(\omega) = [\varepsilon^N_{\mathrm{HOMO}}(\omega) + \mathrm{IP}^N(\omega)]^2 + [\varepsilon^{N+1}_{\mathrm{HOMO}}(\omega) + \mathrm{IP}^{N+1}(\omega)]^2, \quad (3)$$

where $\varepsilon^N_{\mathrm{HOMO}}$ and $\varepsilon^{N+1}_{\mathrm{HOMO}}$ correspond to the energies of the highest occupied molecular orbitals (HOMO) of the N-electron system and N+1-system, respectively, calculated at a given ω. The first part of the Eq. (3) attempts to enforce the ionization potential theorem, where during the OT procedure one strives to obtain the $\varepsilon^N_{\mathrm{HOMO}}$ as close as possible to the IP, determined through the self-consistent field procedure (ΔSCF), *i.e.*,

$$\mathrm{IP}^N(\omega) = E^{N-1}(\omega) - E^N(\omega), \quad (4)$$

$$\mathrm{IP}^{N+1}(\omega) = E^N(\omega) - E^{N+1}(\omega). \quad (5)$$

The second part of the Eq. (3) comes from the fact that in DFT theory, there is no equivalent of the ionization potential theorem for the relation between the electron affinity and the energy of the lowest unoccupied MO (LUMO). Thus, one uses the IP of N+1-system instead of the EA of the N-electron system.[26] In the following, LC-PBE functional that is tuned using the Eq. (3) is referred to as LC-PBE$^{\Delta\mathrm{SCF}}$.

In this work, we also use another way of optimal tuning in which the $\varepsilon^N_{\mathrm{HOMO}}$ and $\varepsilon^N_{\mathrm{LUMO}}$ are fitted to be as near as possible to the *GW* $\varepsilon^{N,GW}_{\mathrm{HOMO}}$ and $\varepsilon^{N,GW}_{\mathrm{LUMO}}$ quasiparticle energies designed to reproduce proper electron removal and addition energies. Namely, we minimize the following equation,

$$J^2(\omega) = [\varepsilon^N_{\mathrm{HOMO}}(\omega) - \varepsilon^{N,GW}_{\mathrm{HOMO}}]^2 + [\varepsilon^N_{\mathrm{LUMO}}(\omega) - \varepsilon^{N,GW}_{\mathrm{LUMO}}]^2. \quad (6)$$

Since both $\varepsilon^{N,GW}_{\mathrm{HOMO}}$ and $\varepsilon^{N,GW}_{\mathrm{LUMO}}$ are defined externally, one only needs to perform calculations for the N-electron system to get the frontier MOs energies at different ω. This means that such an approach is lighter than the conventional OT one, especially important for larger molecules since several iterations with charged systems (N+1 and N-1) are substituted by a single *GW* calculation. A previous comparison of the *GW* and ΔSCF techniques for the IP and EA of medium sized molecular systems invited to favor the *GW* formalism over ΔSCF.[84,85] For sake of exploration, we use here two schemes to perform *GW* calculations: non-self-consistent G_0W_0 and eigenvalue-self-consistent ev*GW* methods.[59,60] The latter is known to be efficient in washing out the starting point (DFT functional) dependency for both energies[49,51] and PES calculations.[62,63] In what follows, the LC-PBE functionals tuned using the Eq. (6) are referred to as LC-PBE^{G_0W_0} or LC-PBE$^{\mathrm{ev}GW}$, depending on the *GW* approach used to determine the IP and EA energies.

B. Computational details

General optimal tuning procedure. In this work, we perform optimal tuning of LC-PBE functional using ΔSCF (conventional OT) and *GW* procedures. The needed DFT calculations have been carried out with the Gaussian16 program[86] thanks to in-house developed code generously provided by S. Sitkiewicz. The range separation parameter is searched between 0.05 and 0.95 a.u. with an accuracy of 0.001 a.u. We report all the ω values obtained for OT functionals in the SI. In the case of OT with *GW*, the HOMO and LUMO quasiparticle energies have been obtained directly from G_0W_0@PBE0 or ev*GW*@PBE0 calculations. The resulting *GW* energy levels have been next plugged into Eq. (6). At the ev*GW* level, we corrected 15 (all for the small molecules) occupied and 15 virtual orbitals for each molecule, higher/lower levels being rigidly shifted following the highest/lowest explicitly corrected level. These calculations have been conducted using the BEDEFT (beyondDFT) package,[87,88] exploiting Coulomb-fitting resolution-of-identity (RI-V) techniques[89] and a robust analytic continuation scheme.[88] The initial DFT calculations are performed with the ORCA 5.1 code.[90]

Set of small molecules. The GS geometries of 10 compact molecules (see Figure 1), for which optimized CC3/*aug*-cc-pVTZ structures are known,[75,91] have been used for the OT procedure and *GW* calculations. We adopted the *aug*-cc-pVTZ atomic basis set for all calculations, together with the corresponding auxiliary basis set for the *GW* runs. The GS and ES geometry optimizations have been performed using the PBE, PBE0, LC-PBE, LC-PBE$^{\Delta\mathrm{SCF}}$, LC-PBE^{G_0W_0}, and LC-PBE$^{\mathrm{ev}GW}$ functionals using Gaussian16 code. The *tight* keyword is set for geometry optimizations, otherwise, default settings are used. We performed frequency analysis to ensure that all the optimized geometries are true minima, except for the ES geometry of molecule **2** that we constrained to have the same point group as in the reference CC calculations. The CC reference values (CC3, CCSD, and CC2 with *aug*-cc-pVTZ atomic basis set) are taken from the Ref. 75 and have been obtained with the linear response (LR) formalism for the ES part. Cartesian coordinates of the optimized structures can be found in the SI.

DMABN. OT and *GW* calculations have been conducted using the CCSD(T)/cc-pVTZ optimized geometries of DMABN (see Figure 1) with 0° and 90° twist angle between dimethylamino group (NMe_2) and phenyl ring, taken from a previous work.[92] We obtained 6 OT functionals: LC-PBE$^{\Delta\mathrm{SCF}\,\omega(0^\circ)}$, LC-PBE$^{G_0W_0\,\omega(0^\circ)}$, LC-PBE$^{\mathrm{ev}GW\,\omega(0^\circ)}$, LC-PBE$^{\Delta\mathrm{SCF}\,\omega(90^\circ)}$, LC-PBE$^{G_0W_0\,\omega(90^\circ)}$, and LC-PBE$^{\mathrm{ev}GW\,\omega(90^\circ)}$, where $\omega(0^\circ)$ or $\omega(90^\circ)$ indicates that OT was done using

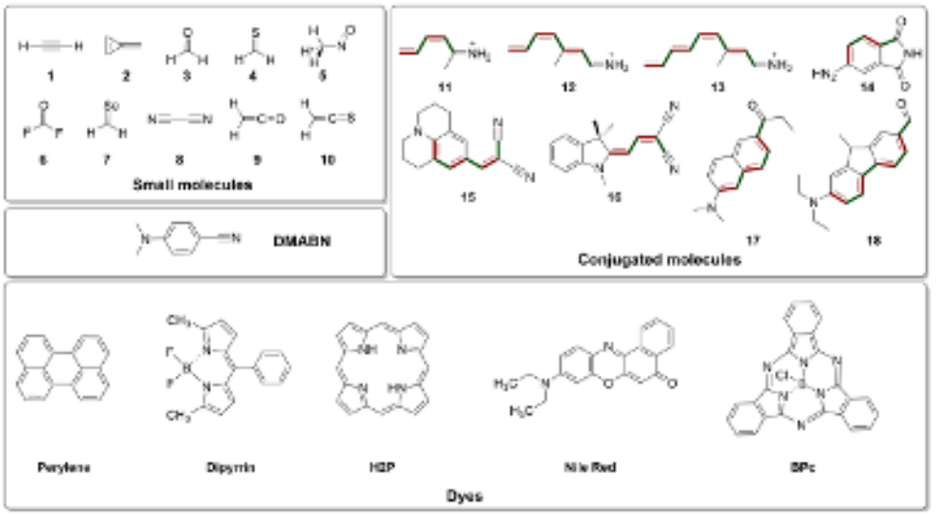

FIG. 1. Structures of the molecules studied in this work. Red (green) indicates the double (single) bonds used for the calculation of the BLA parameter.

the 0° or 90° geometry, respectively. Using these OT functionals, as well as PBE, PBE0, and the not-tuned LC-PBE, we optimized the GS structure as well as the ES geometries for two states corresponding to the local excitation (LE) and CT transitions. These calculations have been done in Gaussian16 code using *tight* criteria for optimizations. We employed the cc-pVDZ basis set in all geometry optimization and frequency calculations since as references, we used the EOM-CCSD/cc-pVDZ geometries optimized in a previous work.[62] Additionally, we have also performed optimization for these states at the LR-CC2/cc-pVDZ level using Turbomole code.[93,94] Cartesian coordinates of the optimized geometries can be found in the SI. The frequency analysis was carried out on all optimized geometries to confirm that they are true minima. We conducted the comparison of the optimized geometries by using as metric the root-mean-square deviation (RMSD), which gives the deviation (in Å) between two superimposed structures **A** and **B** composed of N atoms,

$$\mathrm{RMSD}(\mathbf{a},\mathbf{b}) = \sqrt{\frac{1}{N}\sum_{i=1}^{N}[(a_{ix}-b_{ix})^2+(a_{iy}-b_{iy})^2+(a_{iz}-b_{iz})^2]} \tag{7}$$

where **a** and **b** corresponds to the Cartesian coordinates of molecules **A** and **B**, respectively. This was done using the PyMOL package,[95] where we aligned each of the optimized geometry using the C1, C2, and C3 atoms (see Figure 2) to the reference CCSD/cc-pVDZ structure.

FIG. 2. Structure of the DMABN highlighting the key atoms that were used for structural alignment.

Conjugated molecules. The optimal RI-CC2/*aug*-cc-pVTZ GS geometries of the eight large compounds shown in Figure 1 have been taken from the work of Guido *et al.*[12] and used for the OT procedure and *GW* calculations. All calculations have been performed with the *aug*-cc-pVTZ atomic basis set. The GS and ES structures, constrained to the highest possible point group, were next optimized with PBE, PBE0, LC-PBE, LC-PBE$^{\Delta\mathrm{SCF}}$, LC-PBE^{G_0W_0}, and LC-PBE$^{\mathrm{ev}GW}$ functionals in Gaussian16 code. In this case, following Ref. 12, we compare the bond length alternation (BLA), that is, the difference between the average single and double bond lengths,[96]

$$\mathrm{BLA} = \frac{\sum l_\mathrm{s}}{n_\mathrm{s}} - \frac{\sum l_\mathrm{d}}{n_\mathrm{d}}, \tag{8}$$

where $\sum l_\mathrm{s}$ and $\sum l_\mathrm{d}$ are the sum of the lengths of single and double bonds respectively, and n_s and n_d are the number of single and double bonds. See Figure 1 for the selected bonds.

Dyes. Five dyes were selected (see Figure 1): **Perylene**, N,N'-difluoroboryl-1,9-dimethyl-5-phenydipyrrin (**Dipyrrin**), **H2P**, **Nile Red**, and a boron subphthalocyanine chloride (**BPc**). The def2-SVPD[97] atomic basis set was used in all calculations. The GS optimizations were first achieved with PBE0 functional using the Gaussian16 code. These PBE0 optimized geometries are then adopted for the OT procedure and the *GW* calculations. For the geometry optimizations, in contrast to the previous cases, we added solvent effects with a polarizable continuum model (PCM).[98] The solvents were selected according to the ones used to record the experimental spectra (see the PhotochemCAD$^{\mathrm{TM}}$ database[67]), *i.e.*, cyclohexane for **Perylene**, toluene for **Dipyrrin** and **H2P**, dioxane for **Nile Red**, and benzene for **BPc**. The GS and ES optimizations have been performed using the PBE, PBE0, LC-PBE, LC-PBE$^{\Delta\mathrm{SCF}}$, LC-PBE^{G_0W_0}, and LC-PBE$^{\mathrm{ev}GW}$ functionals with the Gaussian16 code. The minimum structures were confirmed by frequency analysis. The vibrationally resolved spectra were determined with the FC-Classes 3 program.[99,100] We used a TD formalism, applied the

FC approximation (adding HT effects[71,101] for the states with low oscillator strength, *i.e.*, S_1 and S_2 of **H2P**), and selected the so-called Adiabatic Hessian (AH)[66] vibronic model for the band topologies. All vibronic calculations have been performed using internal curvilinear coordinates.[102] During the vibronic calculations, the vibrational contributions, transition energies and dipole moments are coming from PCM-(TD)-DFT. The simulation temperature of 298K was set in all calculations. To reproduce the experimental spectra, a convolution Gaussian function of HWHM of 200 cm^{-1} was used for **Perylene** and **BPc**, 300 cm^{-1} for **Dipyrrin** and **H2P**, and 600 cm^{-1} for **Nile Red**. We focused only on absorption and emission to the first ES, except for **H2P** where we simulated the absorption spectra with contributions from S_1 to S_4 ES. However, we note that with PBE, PBE0, and LC-PBE^{G_0W_0} the optimized structure for the S_3 state could not be obtained, which means that the contribution of this state to the absorption spectra was excluded for these three functionals.

III. RESULTS AND DISCUSSION

A. Evaluating the accuracy of geometrical parameters

In this Section we explore the accuracy provided by OT LC-PBE functionals and compare the results obtained with both standard functionals (PBE and PBE0) and various CC methods (CC2, CCSD, or CC3) for structural parameters: bonds and angles, RMSD, and BLA values. We investigate a large panel of cases going from molecules composed of few atoms to large π-conjugated molecules.

1. Small molecules

Let us start with the results for a set of small molecules (see Figure 1) for which highly accurate CC3 reference values are available. We discuss only the statistical analysis carried out for the bond lengths and valence angles of molecules **1** to **10**, a full list of all parameters is listed in the SI (Tables S2-S5). For acetylene, molecule **1**, we considered three singlet ES of C_{2v} (A_2) and C_{2h} (A_u and B_u) symmetries, while for the remaining molecules, only the lowest singlet was considered (see Figure S1 for details). Although we are mainly focused on ES geometries, let us briefly discuss the statistics for GS geometries as well. In Figures S2 and S3, we present the error distributions for the bond lengths and valence angles of molecules **1** to **10** obtained with CCSD, CC2, PBE, PBE0, LC-PBE, LC-PBE$^{\Delta SCF}$, LC-PBE^{G_0W_0}, and LC-PBE^{evGW} levels using CC3 data as references. First, we notice that both the mean absolute error (MAE) and the standard deviation of the errors (σ) are quite low for both parameters in the GS. Globally, all methods provide rather satisfying results. This is not surprising since molecules **1**-**10** are both small and quite rigid. The highest MAE, 0.016 Å for bond lengths, is obtained with the non-tuned LC-PBE functional, while all the tuned ones deliver smaller errors (Figure S2). In addition, analysing the errors for the GS valence angles, we found that both PBE and PBE0 are less accurate than other methods (Figure S3), whereas they are significantly more accurate for the bond lengths.

In Figures 3 and 4, we now present the error distributions for ES bond lengths and valence angles, respectively. One can notice that when going to the ES, the errors increase as compared to the GS, especially for the valence angles. Interestingly, while in the GS going from PBE to PBE0 results in considerably lower statistical errors for the valence angles, in the ES both methods deliver roughly equivalent accuracies. Moreover, the largest MAE and σ are obtained with the standard LC-PBE functional for both structural parameters. Optimal tuning improves the accuracy of the LC-PBE functional, especially for valence angles, where the lowest errors in the OT series are obtained with LC-PBE^{G_0W_0}. In the case of CC methods, we can notice that even though both CC2 and CCSD provide very accurate bond lengths in both the GS and ES, CC2 provide ES valence angles closer to the CC3 reference values than CCSD.

Additionally, we also computed the linear determination coefficient (R^2). The correlation graphs for parameters and methods discussed in this Section are given in Figures S4-S7. One can see a nearly perfect correlation between the structural parameters in the GS. As expected from the discussion above, the ES R^2 values, especially for angles, are lower for all studied methods, even though we still observe high correlations with the CC3 reference data.

It is also interesting to look at the error distributions for various bond (or angle) types. In the distribution of GS and ES bond lengths (Figure S2 and 3), one can spot that C-H and C-C bond lengths are usually accurately reproduced by all methods. Let us now focus on outliers: LC-PBE tends to underestimate quite strongly both C=Se and C=S bond distances, in both GS and ES as compared to CC3 values (with an error of *ca.* -0.04 Å in GS and *ca.* -0.09 Å in the ES). OT efficiently lowers the LC-PBE errors for these bond lengths and generally improves the accuracy. We note that even CCSD tends to underestimate these bond lengths in the ES. Furthermore, one more challenging ES bond is the C=O bond, an unsurprising fact on the basis of previous analysis.[75,103] While CCSD underestimates the C=O bond distance, CC2 behaves oppositely, providing too stretched bonds as compared to CC3. Similarly to the previous case, LC-PBE provides the largest underestimation among all tested methods. Surprisingly, OT functionals do not significantly improve the estimate for the C=O bond length. Considering now the angles (Figures S3 and 4) one notices that both GS and ES structures optimized with PBE, PBE0, and LC-PBE have a common outlier, that is the C-N=O angle of molecule **5**. Both LC-PBE$^{\Delta SCF}$ and LC-PBE^{G_0W_0} offer slight reduction of the error for this angle. Additionally, there are two other significant errors with the LC-PBE functional related to the C≡C-H and C=C=S angles, yet these errors can be effectively reduced using OT. These angles are also too open with CCSD.

To conclude, all methods tend to provide quite accurate bond lengths in both GS and ES for the molecules composed of a few atoms with C=O and C=S ES bonds being challenging. However, it is more challenging to get accurate valence angles even in the GS. The LC-PBE functional is the least

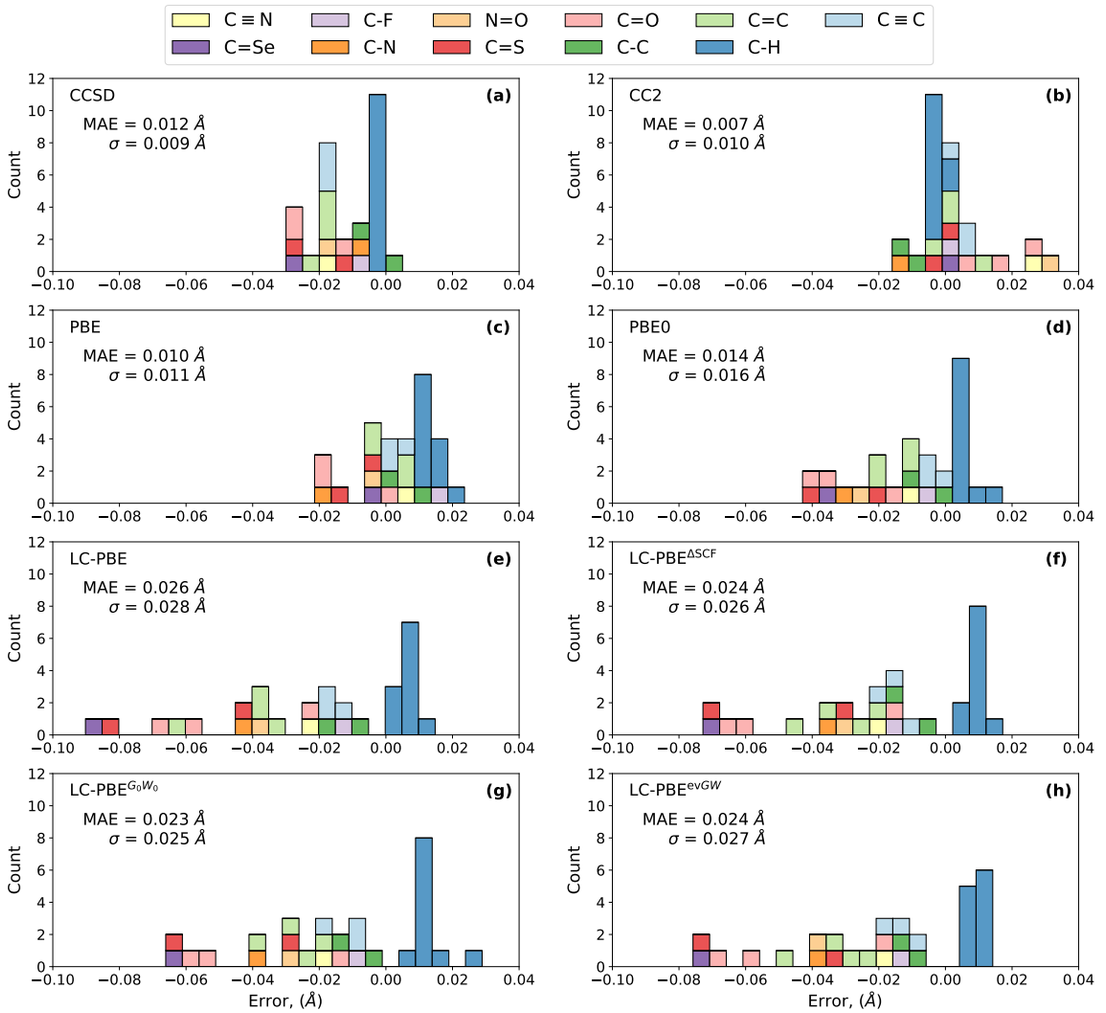

FIG. 3. Histogram showing ES bond length error distributions for the set of 10 small molecules obtained with (a) CCSD, (b) CC2, (c) PBE, (d) PBE0, (e) LC-PBE, (f) LC-PBE$^{\Delta\text{SCF}}$, (g) LC-PBE^{G_0W_0}, and (h) LC-PBE$^{\text{ev}GW}$ methods as compared to CC3 reference values. All calculations are done with the *aug*-cc-pVTZ atomic basis set. MAE and σ are in Å.

accurate of our set and OT can be a way to reduce these errors, especially when using the LC-PBE^{G_0W_0} functional. However, neither approach would clearly outperform traditional DFT/TD-DFT for such compact compounds. This is at odds with a previous work where for carbon monoxide, acetone, acrolein, and methylenecyclopropene, BSE/G_0W_0 and BSE/ev*GW* ES geometries (numerical gradients) were found to be more accurate than those obtained with standard TD-DFT calculations performed with PBE0, M06-2X, and CAM-B3LYP functionals.[61] That is why we decided to make a short comparison between our *GW*-tuned LC-PBE ES geometries and the ones obtained with BSE/*GW* numerical gradients. We chose the acetone in C_s symmetry ($n \rightarrow \pi$ lowest singlet ^{1}A" ES) for this purpose. Optimal tuning and ES geometry optimizations were performed using the same cc-pVTZ atomic basis set as in Ref. 61. The results of these calculations are listed in Table I. In agreement with the above discussion, *GW*-tuned functionals provide quite underestimated C=O bond distances and overestimated C-C-C valence angles. In contrast, BSE/*GW* (numerical) estimations are significantly closer to the reference CASPT2 values for that specific case. Nevertheless, quite accurate C-C bond lengths and H-C-C=O dihedrals are provided by *GW*-tuned LC-PBE functionals. Moreover, one may notice that both LC-PBE^{G_0W_0} and LC-PBE$^{\text{ev}GW}$ follow the BSE/*GW* numerical trends, i.e., the non-self-consistent *GW* approach yields more accurate results. Based on this specific example, one may conclude that TD-DFT based on OT functionals do not fully share the accuracy of BSE/*GW* calculations, especially for the description of the polar C=O bond distances and valence angles. This further stresses the importance of the development of actual BSE/*GW* analytical gradients.

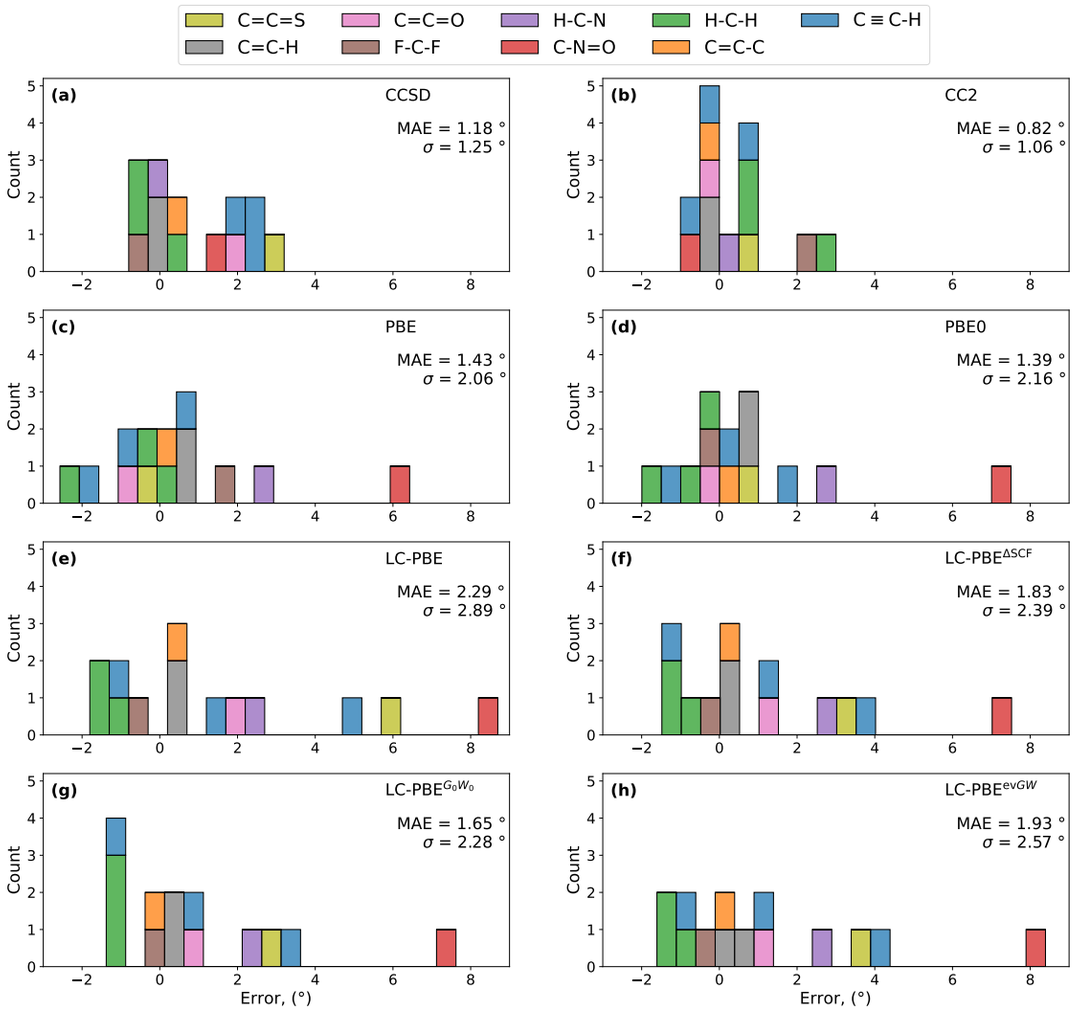

FIG. 4. Histogram showing ES valence angle error distributions for the set of 10 small molecules obtained with (a) CCSD, (b) CC2, (c) PBE, (d) PBE0, (e) LC-PBE, (f) LC-PBE$^{\Delta SCF}$, (g) LC-PBE^{G_0W_0}, and (h) LC-PBE^{evGW} methods as compared to CC3 reference values. All calculations are done with *aug*-cc-pVTZ atomic basis set. MAE and σ are in degrees.

TABLE I. Calculated values of the optimized C=O and C-C bond lengths, C-C-C valence angle and H-C-C=O dihedral of $n \rightarrow \pi$ lowest singlet ^{1}A" ES in acetone in C_s symmetry. CASPT2, BSE/G_0W_0 (numerical) and BSE/evGW (numerical) values have been taken from Ref. 61. All calculations rely on the cc-pVTZ atomic basis set.

Method	C=O, [Å]	C-C, [Å]	C-C-C, [°]	H-C-C=O, [°]
CASPT2	1.350	1.496	112.75	52.25
BSE/G_0W_0 (numerical)	1.327	1.495	113.63	49.83
BSE/evGW (numerical)	1.302	1.504	114.58	50.09
LC-PBE^{G_0W_0}	1.293	1.490	120.55	53.14
LC-PBE^{evGW}	1.283	1.491	120.16	52.11

2. *Excited state DMABN geometries*

Let us now consider a larger and more challenging structure, DMABN. The interest in this molecule lies in its peculiar photophysics, *i.e.*, dual fluorescence. This phenomenon usually occurs in polar solvents, where one can observe two emission bands: a high energy peak originating from a LE state and a low energy band assigned to the intramolecular CT state. The reason behind this phenomenon is the twisted intramolecular charge transfer (TICT) mechanism,[104] where the CT structure in which the NMe_2 group is perpendicular to the benzene ring can be stabilized in the polar environment.[105,106] Here we are comparing the accuracy of the optimized geometries for both LE and CT states of DMABN using DFT functionals (PBE, PBE0, LC-PBE) as well as LR-CC2 selecting the EOM-CCSD geometries of Ref. 62 as reference. We test the performance of six LC-PBE functionals tuned on 0° and 90° structures: LC-PBE$^{\Delta SCF}\omega(0^\circ)$, LC-PBE$^{G_0W_0}\omega(0^\circ)$, LC-PBE$^{evGW}\omega(0^\circ)$, LC-PBE$^{\Delta SCF}\omega(90^\circ)$, LC-PBE$^{G_0W_0}\omega(90^\circ)$, and LC-PBE$^{evGW}\omega(90^\circ)$. In order to compare the obtained optimized geometries efficiently, we aligned the structures (as described in the Computational details section) and computed the RMSD values with respect to the EOM-CCSD structures.

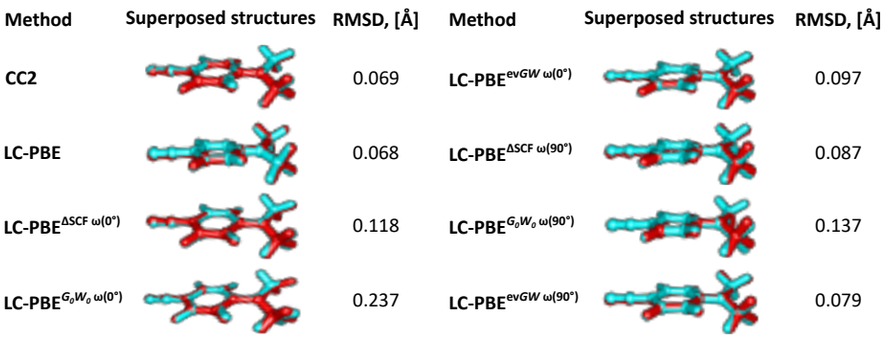

FIG. 5. Superposition of the optimized structures obtained with different methods as compared to the EOM-CCSD reference geometry for the LE state of DMABN. RMSD values are listed. The results have been obtained with the cc-pVDZ atomic basis set. The red-coloured structure corresponds to the reference CCSD/cc-pVDZ optimized geometry.

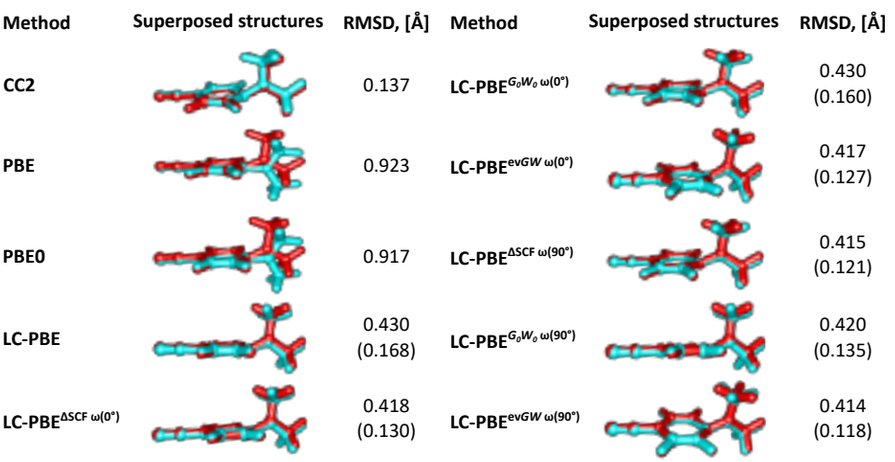

FIG. 6. Superposition of the optimized CT structures obtained with different methods as compared to the EOM-CCSD reference geometry. RMSD values in brackets have been calculated omitting the three hydrogen atoms of the NMe_2 group "above" the phenyl ring. See the caption of Figure 5 for more details.

In Figure 5 we present the superposed structures for the LE state obtained with all methods studied in this Section (in blue) compared to the reference EOM-CCSD geometry (in red). As one notices, we are not reporting the structures obtained with PBE and PBE0 functionals. This is simply due to the fact that these two functionals twist the structures (up to ca. 90^o, during the minimization, leading to minima that cannot be directly compared to the ones obtained with EOM-CCSD. Such behaviour of the PBE and PBE0 stems from the known underestimation of the CT energies by these functionals,[15,16] and was reported before with PBE for DMABN.[17] One can notice that both CC2 and LC-PBE nicely match the CCSD geometry with an RMSD of *ca.* 0.07 Å. OT functionals such as LC-PBE$^{\Delta SCF}$ and LC-PBE^{G_0W_0} tuned on untwisted structure ($\omega(0^\circ)$) lead to significantly higher RMSD values. In contrast, the same functionals but tuned on the 90° structure deliver more accurate results as compared to the CCSD reference. This is a rather surprising result since the LE minimum at the EOM-CCSD level has a twist angle of *ca.* 18°, which is closer to the untwisted structure than the 90° twisted geometry. There are likely some error compensation taking place here. We highlight that for the LE state, LC-PBE^{evGW} provides the best agreement, among OT functionals, with the reference values nearly independent of the DMABN geometry (untwisted or twisted) used for the tuning procedure, which confirms the quality of the ev*GW* estimates.

In Figure 6, we present the optimized structures obtained with TD-DFT (PBE, PBE0, LC-PBE, and OT LC-PBE) and CC2 levels aligned to the EOM-CCSD results for the CT ES. First, CC2 provides a structure in good agreement with the CCSD reference. In contrast, PBE and PBE0, which wrongly predict this ES to be more stable than its LE counterpart, show very large RMSD. This is because PBE and PBE0 predict the NMe_2 group to be strictly perpendicular to the benzene ring, whereas all other methods yield pyramidalization of the amino group and thus a smaller twist angle. The situation is improved with all LC-PBE variants, an expected outcome for a CT structure. Nevertheless, for both the non-tuned and tuned LC-PBE functionals, the RMSD are significantly higher than the ones for the LE state. We see that for CT geometries all the OT functionals, no matter on which structures they are tuned, provide similar RMSD values in the 0.41–0.43 Å range.

Looking more carefully at the superposed structures in Figure 6, one can see that these differences are coming from rotations of one of the methyl groups as compared to CCSD. Omitting the three problematic hydrogen atoms, OT functionals provide more accurate ES geometries than the ones obtained with LC-PBE. In addition, LC-PBE^{evGW} $\omega(90^\circ)$ provides the lowest RMSD among OT functionals, which makes good sense since the tuning was performed on a twisted structure with a self-consistent *GW* scheme.

In the previous Section, we have seen that both PBE and PBE0 deliver quite accurate structural parameters for small molecules. Here, we see that they are failing to provide the LE minimum and provide inaccurate geometries of the CT state. On balance, LC-PBE^{evGW} tuned on the 90° structure delivers the most satisfying geometries, although the CT structure differs a bit from the CCSD reference due to the rotation of one methyl group. However, it is fair to say that the tuning scheme, using either ΔSCF or *GW* removal energies, does not lead to a dramatic increase of accuracy as compared to the untuned LC-PBE functional.

3. *Conjugated molecules*

In the previous Sections we discussed the structural differences between optimized structures obtained at various levels of theory. Here, we are going to investigate how these geometrical differences can be linked to the character of the ES. It is first important to note that compounds **11** – **13** have a partial cyanine nature. Indeed cyanine ES are known to be especially challenging for TD-DFT[107–109] but less so for BSE/*GW*.[48] Following Ref. 12 we used the BLA parameter (see Computational details Section), which is the difference between the average single and double bond lengths along a conjugation path, as a metric to assess methodological aspects. Based on the value of the BLA one can qualitatively split the system or state into "neutral" (BLA > 0), "delocalized" (or cyanine-like, BLA around 0), and "charge-transfer" (BLA < 0).[12]

In Figure 7 we present ES BLA values obtained for molecules **11** – **18** (see Figure 1) using CC2, PBE, PBE0, LC-PBE, LC-PBE$^{\Delta SCF}$, LC-PBE^{G_0W_0}, and LC-PBE^{evGW} levels of theory. As one may notice for PBE we only report the values for molecules **11** – **13**, as for other molecules the ES optimization did not converge, which is unsurprising given their clear CT structure. Additionally, the PBE0 optimized ES structure of **15** displays an out-of-plane ethenyl bridging moiety, *i.e.*, the conjugation path is broken and we cannot calculate a relevant BLA value in that case. PBE and PBE0 are quite far from the CC2 reference and provide quite overestimated BLA values, especially for the ES of the cyanine derivatives **11** to **13**. In contrast, LC-PBE tends to underestimate the reference BLA values, except in a few cases. In general, we can see that OT functionals are in good agreement with the reference CC2 values, the match being nearly perfect for the three cyanine systems. Indeed, significant improvement over LC-PBE results can be obtained by using optimal tuning for most of the molecules studied. For the largest molecule in the set, **18**, LC-PBE predicts a more neutral character for this ES, while

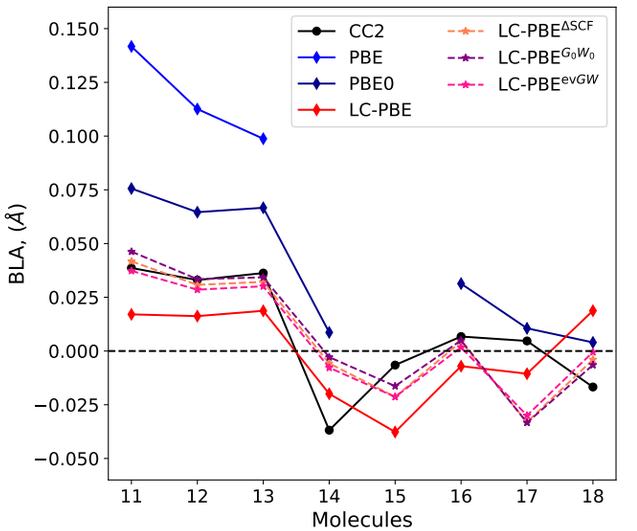

FIG. 7. Excited-state BLA values for molecules **11** – **18** calculated with DFT and CC2 levels of theory using *aug*-cc-pVTZ. The CC2 values have been taken from Ref. 12.

OT functionals provide lower BLA values closer to the small CT character foreseen by CC2. However, a few problematic cases can be detected as well such as molecule **14** and **17**. In these two cases, the optimal tuning leads to BLA values further from the reference. Guido *et al.*[12] rationalized the large discrepancy between the CC2 and RSH (CAM-B3LYP) geometries for molecule **14** by the double excitation character for this ES, a feature that cannot be efficiently captured by TD-DFT nor BSE/*GW*.

In most cases, the OT functionals, regardless of the scheme used for tuning, can provide quite accurate BLA values and significantly improve the LC-PBE results.

B. Modelling of the absorption and emission spectra: 0-0 energies and band shapes

Now we turn towards the comparison of the absorption and fluorescence spectral data. As we highlighted in the Introduction, it is a way to compare the computed ES geometries and PES to experiments. We first discuss 0-0 energies, a parameter that can be quite easily determined from the intersection of absorption and emission spectra measured in solution.[110–113] One can directly calculate 0-0 energies by adding the difference of zero-point vibrational energy (ZPVE) between ES ($E_{\rm ES}^{\rm ZPVE}$, determined at ES geometry) and GS ($E_{\rm GS}^{\rm ZPVE}$, determined at GS geometry) to the adiabatic energy

$$E^{0-0} = E^{\rm adia} + \Delta E^{\rm ZPVE} = \left(E_{\rm ES}^{\rm ES} - E_{\rm GS}^{\rm GS}\right) + \left(E_{\rm ES}^{\rm ZPVE} - E_{\rm GS}^{\rm ZPVE}\right),$$

where $E_{\rm ES}^{\rm ES}$ and $E_{\rm GS}^{\rm GS}$ are ES and GS total energies determined at their respective minimal geometries. The comparison of 0-0 energies between experiment and theory is preferred over the use of theoretically calculated vertical energies, since the experiment is not a purely vertical process.[10,112,114–117] In Table

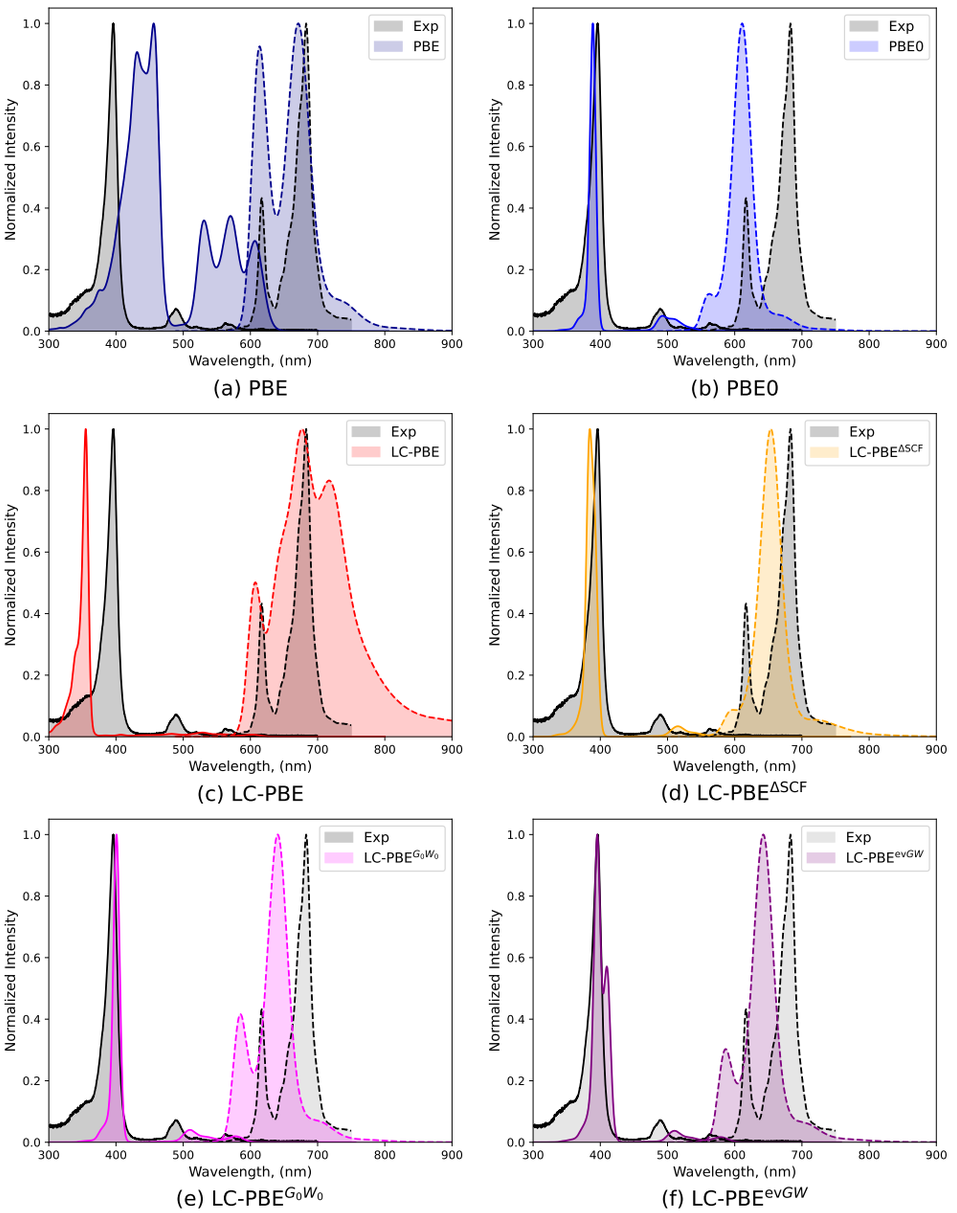

FIG. 8. Normalized vibronically-resolved absorption (solid line) and fluorescence (dashed line) spectra of **H2P** calculated with (a) PBE, (b) PBE0, (c) LC-PBE, (d) LC-PBE$^{\Delta SCF}$, (e) LC-PBE^{G_0W_0}, and (f) LC-PBE^{evGW} levels of theory compared to the experimental data taken from the PhotochemCAD^{TM} database[67].

II we present experimental 0-0 energies and theoretically estimated ones using PBE, PBE0, LC-PBE, LC-PBE$^{\Delta SCF}$, LC-PBE^{G_0W_0}, and LC-PBE^{evGW} levels of theory. The results show that PBE tends to underestimate the measured 0-0 energies, especially for **Perylene** and **Nile Red**. It is no surprise that a semilocal functional yields too small transition energies for organic molecules. In contrast, PBE0 usually overestimates reference values, except for **Perylene**. The mean absolute error (MAE) obtained with PBE0, *ca.* 0.2 eV's, typical of this level of theory.[112] Similarly to PBE0, LC-PBE generally shows an overestimation trend but with somewhat larger error, *e.g.*, a significantly large difference as compared to the experiment is seen for **Nile Red**. Even though OT functionals also overestimate 0-0 energies, except for **Perylene**, they are usually closer to the experimental values than other methods. For "traditional" OT functionals this finding is consistent with literature precedent[27,29] and we show here that tuning of the *GW* energies is as successful. It seems like **Perylene** and **Nile Red** 0-0 energies are the most challenging cases for theoretical methods to reproduce. Nevertheless, it is clear from Table II that OT functionals provide the most accurate 0-0 energies with the lowest MAE.

TABLE II. 0-0 energies calculated with PBE, PBE0, LC-PBE, LC-PBE$^{\Delta SCF}$, LC-PBE^{G_0W_0}, and LC-PBE^{evGW} methods compared to the experimental energies. Energies and MAE are in eV.

	Exp	PBE	PBE0	LC-PBE	LC-PBE$^{\Delta SCF}$	LC-PBE^{G_0W_0}	LC-PBE^{evGW}
Perylene	2.87	2.23	2.52	3.07	2.67	2.56	2.62
Dipyrrin	2.43	2.45	2.65	2.71	2.58	2.55	2.57
H2P	2.13	2.04	2.24	2.05	2.11	2.14	2.14
Nile Red	2.24	1.77	2.41	2.82	2.40	2.33	2.40
BPc	2.16	2.10	2.27	2.24	2.26	2.23	2.25
MAE		0.26	0.19	0.24	0.12	0.12	0.13

Let us now move to a comparison of the experimental and theoretical band topologies. We present the vibronically-resolved absorption and fluorescence spectra in Figures S8-S17. One can see that generally the spectral shapes are quite well reproduced by all tested methods. However, both PBE and PBE0 functionals quite often provide either overestimated or underestimated molar extinction coefficients (ε) for the absorption process (see Figure S8-S12). Furthermore, the PBE ε value for **Nile Red** is close to zero (see Figure S11), which is totally incorrect, and this issue is related to the CT nature of the transition. LC-PBE tends to provide more resolved spectra than experimental ones, especially for **Perylene**, where the intensities of the peaks are quite far from the reference (see Figure S8). OT functionals, especially LC-PBE^{G_0W_0} and LC-PBE^{evGW}, yield spectra in quite good agreement with the reference ones in terms of shapes, intensities, and peaks wavelengths. In Figure 8 we present the normalized absorption and fluorescence spectra for **H2P** molecule. We decided to discuss in more detail this case since the absorption spectra includes a contribution from multiple ES and absorption to the first ES has a very low oscillator strength contrary to other dyes. To simulate the absorption spectra of **H2P**, we calculated contributions from four ES and included HT effects for the two lowest ES. One can notice in Figure 8a that the relative peak intensities of PBE are not fitting the experimental ones for both absorption and emission. Additionally, one can see in Figure S9 that the PBE ε values are significantly lower than the reference ones. In contrast, other functionals, especially LC-PBE and LC-PBE$^{\Delta SCF}$, tend to overestimate the ε values, but the best agreement with experimental values is clearly obtained with LC-PBE^{G_0W_0} and LC-PBE^{evGW} (see Figure S10). LC-PBE quite strongly blueshifts the absorption spectra as compared to other functionals. Moreover, the fluorescence spectrum modelled with LC-PBE is significantly broader than the experimental one. OT functionals improve the band shapes, although a slight blueshift pertains for the fluorescence spectrum. Among the OT series, LC-PBE^{G_0W_0} and LC-PBE^{evGW} provide more accurate shapes of both absorption and emission spectra than LC-PBE$^{\Delta SCF}$.

To summarize, OT functionals show significant improvements over the parent LC-PBE functional for the calculation of the spectroscopic properties. More interestingly, LC-PBE^{G_0W_0} and LC-PBE^{evGW} deliver 0-0 energies as well as band shapes and intensities closer to the measured one that the other tested functionals. It is already known that BSE/*GW*, especially using ev*GW* scheme, can provide accurate 0-0 energies.[49] Here, we also show that *GW*-tuned RSH functionals can provide accurate band shapes and intensities for the absorption and emission spectra, which hints at an improved description of the PES around the GS and ES minima.

IV. CONCLUSIONS

In this contribution, we assessed the accuracy of ES geometries obtained with optimally-tuned (OT) LC-PBE functionals, tuned on the IP and EA obtained with the *GW* approach, *i.e.*, LC-PBE^{G_0W_0} and LC-PBE^{evGW}. We investigated the ES optimization with these functionals and compared the results to standard DFT (PBE and PBE0), conventionally tuned (LC-PBE$^{\Delta SCF}$), and non-tuned LC-PBE functionals. We provided comparisons of the ES geometries to high-level CC reference values as well as experimental data.

In the first part, we investigated the performance of the *GW*-tuned OT functionals for three different types of systems including molecules composed of few atoms, DMABN, and conjugated dyes. For the few-atoms compact systems, there is no clear advantage over standard TD-DFT. This differs from the results of a previous work relying on BSE/*GW* finite-difference calculations,[61] suggesting that tuned LC-functionals, even when tuning is performed on *GW* removal energies, cannot capture all the features of the many-body formalism. In contrast, in the case of DMABN for which PBE and PBE0 fail, LC-PBE^{evGW} tends to deliver the closest agreement with reference EOM-CCSD geometries independently of the DMABN geometry used for the tuning procedure. For large cyanine and push-pull systems, all OT functionals provide similar results, showing significant improvements over the non-tuned LC-PBE functional. Finally, we also compared the theoretical and experimental spectra as a metric to evaluate the accuracy of the ES geometries and PES around the optimal geometry. The obtained results suggest that *GW* tuned LC-PBE functionals not only provide accurate 0-0 energies but are also more likely to deliver the accurate band shapes and intensities for the absorption and emission spectra. Additionally, we highlight that in the case of large dyes, the computational costs of *GW* tuning can be noticeably lower as compared to the conventional tuning.

We have shown that the tuning of RSH functionals on *GW* quasiparticle energies can be beneficial to improve TD-DFT excited state geometries, especially in the case of larger dye molecules. However, this improvement cannot be viewed as systematic, since no gain is obtained for, e.g., small compounds. We hope that our work will be an additional stimulus for the scientific community to focus on the development of efficient techniques for obtaining BSE/*GW* analytic gradients in both gas and condensed phases.

Supplementary Material

See the supplementary material for OT ω values, raw data, additional statistical analyses for all sets, as well as additional absorption and emission spectra for the dyes.

ACKNOWLEDGMENTS

All the authors are thankful for the in-house developed code to perform the optimal tuning procedure generously provided by S. Sitkiewicz. We are also grateful to C.A. Guido for providing CC2 optimized structures for compounds **11** – **18**. This work is supported by the French Agence Nationale de la Recherche (ANR) under contract ANR-20-CE29-0005 (BSE-Forces). This work received financial assistance from the State within the framework of the EUR LUMOMAT project and the Investissements d'Avenir program ANR-18-EURE-0012. We are thankful to the CCIPL (GLiCID) computational center installed in Nantes and the national HPC facilities under contract GENCI-TGCC A0110910016 for the generous allocation of the computational resources.

Author Declarations

Conflict of Interest

The authors have no conflicts to disclose.

[1]H. Uoyama, K. Goushi, K. Shizu, H. Nomura, and C. Adachi, Nature **492**, 234 (2012).
[2]W. Sun, S. Guo, C. Hu, J. Fan, and X. Peng, Chem. Rev. **116**, 7768 (2016).
[3]T. Terai and T. Nagano, Curr. Opin. Chem. Biol. **12**, 515 (2008).
[4]Y. Xu, P. Zhang, A. Gao, R. Xu, Z. Wang, Q. Shen, Z. Zhao, L. Meng, and D. Dang, Mater. Chem. Front. **7**, 828 (2023).
[5]D. J. Clouthier and D. A. Ramsay, Annu. Rev. Phys. Chem. **34**, 31 (1983).
[6]T. Huet, M. Godefroid, and M. Herman, J. Mol. Spectrosc. **144**, 32 (1990).
[7]M. E. Köse, ACS Omega **7**, 32764 (2022).
[8]E. Runge and E. K. U. Gross, Phys. Rev. Lett. **52**, 997 (1984).
[9]M. E. Casida, "Time-dependent density functional response theory for molecules," in *Recent Advances in Density Functional Methods*, Vol. 1, edited by D. P. Chong (World Scientific: Singapore, 1995) pp. 155–192.
[10]C. Adamo and D. Jacquemin, Chem. Soc. Rev. **42**, 845 (2013).
[11]C. A. Guido, D. Jacquemin, C. Adamo, and B. Mennucci, J. Phys. Chem. A **114**, 13402 (2010).
[12]C. A. Guido, S. Knecht, J. Kongsted, and B. Mennucci, J. Chem. Theory Comput. **9**, 2209 (2013).
[13]A. D. Laurent and D. Jacquemin, Int. J. Quantum Chem. **113**, 2019 (2013).
[14]J. Wang and B. Durbeej, J. Comput. Chem. **41**, 1718 (2020).
[15]D. J. Tozer, J. Chem. Phys. **119**, 12697 (2003).
[16]A. Dreuw and M. Head-Gordon, J. Am. Chem. Soc. **126**, 4007 (2004).
[17]P. Wiggins, J. A. G. Williams, and D. J. Tozer, J. Chem. Phys. **131**, 091101 (2009).
[18]A. Savin, in *Recent Developments and Applications of Modern Density Functional Theory*, Theoretical and Computational Chemistry, Vol. 4, edited by J. Seminario (Elsevier, 1996) pp. 327–357.
[19]H. Iikura, T. Tsuneda, T. Yanai, and K. Hirao, J. Chem. Phys. **115**, 3540 (2001).
[20]T. Yanai, D. P. Tew, and N. C. Handy, Chem. Phys. Lett. **393**, 51 (2004).
[21]J.-D. Chai and M. Head-Gordon, Phys. Chem. Chem. Phys. **10**, 6615 (2008).
[22]É. Brémond, Á. J. Pérez-Jiménez, J. C. Sancho-García, and C. Adamo, J. Chem. Phys. **150**, 201102 (2019).
[23]R. Baer, E. Livshits, and U. Salzner, Annu. Rev. Phys. Chem. **61**, 85 (2010).
[24]T. Stein, H. Eisenberg, L. Kronik, and R. Baer, Phys. Rev. Lett. **105**, 266802 (2010).
[25]J. D. Gledhill, M. J. G. Peach, and D. J. Tozer, J. Chem. Theory Comput. **9**, 4414 (2013), https://doi.org/10.1021/ct400592a.
[26]L. Kronik, T. Stein, S. Refaely-Abramson, and R. Baer, J. Chem. Theory Comput. **8**, 1515 (2012).
[27]B. I. Moore, A. Charaf-Eddin, A. Planchat, C. Adamo, J. Autschbach, and D. Jacquemin, J. Chem. Theory Comput. **10**, 4599 (2014).
[28]J. Autschbach and M. Srebro, Acc. Chem. Res. **47**, 2592 (2014).
[29]D. Jacquemin, B. I. Moore, A. Planchat, C. Adamo, and J. Autschbach, J. Chem. Theory Comput. **10**, 1677 (2014).
[30]T. Körzdörfer and J.-L. Brédas, Acc. Chem. Res. **47**, 3284 (2014).
[31]J. Eng, B. A. Laidlaw, and T. J. Penfold, J. Comput. Chem. **40**, 2191 (2019).
[32]P. Besalú-Sala, S. P. Sitkiewicz, P. Salvador, E. Matito, and J. M. Luis, Phys. Chem. Chem. Phys. **22**, 11871 (2020).
[33]C.-W. Ju, E. J. French, N. Geva, A. W. Kohn, and Z. Lin, J. Phys. Chem. Lett. **12**, 9516 (2021).
[34]E. E. Salpeter and H. A. Bethe, Phys. Rev. **84**, 1232 (1951).
[35]G. Csanak, H. Taylor, and R. Yaris, in *Advances in Atomic and Molecular Physics*, Advances in Atomic and Molecular Physics, Vol. 7, edited by D. Bates and I. Esterman (Academic Press, 1971) pp. 287–361.
[36]G. Strinati, Riv. del Nuovo Cim. **11**, 1 (1988).
[37]M. Rohlfing and S. G. Louie, Phys. Rev. Lett. **81**, 2312 (1998).
[38]S. Albrecht, L. Reining, R. Del Sole, and G. Onida, Phys. Rev. Lett. **80**, 4510 (1998).
[39]L. X. Benedict, E. L. Shirley, and R. B. Bohn, Phys. Rev. Lett. **80**, 4514 (1998).
[40]X. Blase, I. Duchemin, D. Jacquemin, and P.-F. Loos, J. Phys. Chem. Lett. **11**, 7371 (2020).
[41]L. Hedin, Phys. Rev. **139**, A796 (1965).
[42]M. S. Hybertsen and S. G. Louie, Phys. Rev. B **34**, 5390 (1986).
[43]R. W. Godby, M. Schlüter, and L. J. Sham, Phys. Rev. B **37**, 10159 (1988).
[44]D. Golze, M. Dvorak, and P. Rinke, Front. Chem. **7**, 377 (2019).
[45]I. Duchemin, T. Deutsch, and X. Blase, Phys. Rev. Lett. **109**, 167801 (2012).
[46]B. Baumeier, D. Andrienko, and M. Rohlfing, J. Chem. Theory Comput. **8**, 2790 (2012).
[47]P. Cudazzo, M. Gatti, A. Rubio, and F. Sottile, Phys. Rev. B **88**, 195152 (2013).
[48]P. Boulanger, D. Jacquemin, I. Duchemin, and X. Blase, J. Chem. Theory Comput. **10**, 1212 (2014).
[49]D. Jacquemin, I. Duchemin, and X. Blase, J. Chem. Theory Comput. **11**, 3290 (2015).
[50]V. Ziaei and T. Bredow, J. Chem. Phys. **145**, 174305 (2016).
[51]D. Jacquemin, I. Duchemin, and X. Blase, J. Phys. Chem. Lett. **8**, 1524 (2017).
[52]X. Blase, I. Duchemin, and D. Jacquemin, Chem. Soc. Rev. **47**, 1022 (2018).
[53]X. Gui, C. Holzer, and W. Klopper, J. Chem. Theory Comput. **14**, 2127 (2018).
[54]N. C. Handy and H. F. Schaefer, J. Chem. Phys. **81**, 5031 (1984).
[55]J. Villalobos-Castro, I. Knysh, D. Jacquemin, I. Duchemin, and X. Blase, J. Chem. Phys. **159**, 024116 (2023), https://pubs.aip.org/aip/jcp/article-pdf/doi/10.1063/5.0156687/18037481/024116_1_5.0156687.pdf.
[56]S. Ismail-Beigi and S. G. Louie, Phys. Rev. Lett. **90**, 076401 (2003).
[57]M. S. Kaczmarski and M. Rohlfing, J. Phys. B: At. Mol. Opt. Phys. **43**, 051001 (2010).
[58]M. S. Kaczmarski, Y. Ma, and M. Rohlfing, Phys. Rev. B **81**, 115433 (2010).
[59]F. Kaplan, M. E. Harding, C. Seiler, F. Weigend, F. Evers, and M. J. van Setten, J. Chem. Theory Comput. **12**, 2528 (2016).
[60]T. Rangel, S. M. Hamed, F. Bruneval, and J. B. Neaton, J. Chem. Theory Comput. **12**, 2834 (2016).
[61]O. Çaylak and B. Baumeier, J. Chem. Theory Comput. **17**, 879 (2021).
[62]I. Knysh, I. Duchemin, X. Blase, and D. Jacquemin, J. Chem. Phys. **157**, 194102 (2022).
[63]I. Knysh, K. Letellier, I. Duchemin, X. Blase, and D. Jacquemin, Phys. Chem. Chem. Phys. **25**, 8376 (2023).
[64]M. Dierksen and S. Grimme, J. Phys. Chem. A **108**, 10225 (2004).
[65]F. Muniz-Miranda, A. Pedone, G. Battistelli, M. Montalti, J. Bloino, and V. Barone, J. Chem. Theory Comput. **11**, 5371 (2015).
[66]F. Santoro and D. Jacquemin, WIREs Comput. Mol. Sci. **6**, 460 (2016).
[67]M. Taniguchi and J. S. Lindsey, Photochem. Photobiol. **94**, 290 (2018).
[68]F. Egidi, D. B. Williams-Young, A. Baiardi, J. Bloino, G. Scalmani, M. J. Frisch, X. Li, and V. Barone, J. Chem. Theory Comput. **13**, 2789 (2017).

[69]S. Sitkiewicz, E. Matito, J. M. Luis, and R. Zalesny, Phys. Chem. Chem. Phys. , (2023).
[70]F. J. Avila Ferrer and F. Santoro, Phys. Chem. Chem. Phys. **14**, 13549 (2012).
[71]M. H. E. Bousquet, T. V. Papineau, K. Veys, D. Escudero, and D. Jacquemin, J. Chem. Theory Comput. **19**, 5525 (2023).
[72]T. Stein, L. Kronik, and R. Baer, J. Am. Chem. Soc. **131**, 2818 (2009).
[73]B. Kretz and D. A. Egger, J. Chem. Theory Comput. **17**, 357 (2021).
[74]C. A. McKeon, S. M. Hamed, F. Bruneval, and J. B. Neaton, J. Chem. Phys. **157**, 074103 (2022).
[75]S. Budzák, G. Scalmani, and D. Jacquemin, J. Chem. Theory Comput. **13**, 6237 (2017).
[76]O. Christiansen, H. Koch, and P. Jørgensen, Chem. Phys. Lett. **243**, 409 (1995).
[77]J. P. Perdew, K. Burke, and M. Ernzerhof, Phys. Rev. Lett. **78**, 1396 (1997).
[78]C. Adamo and V. Barone, J. Chem. Phys. **110**, 6158 (1999).
[79]G. D. Purvis and R. J. Bartlett, J. Chem. Phys. **76**, 1910 (1982).
[80]H. Koch, H. J. A. Jensen, P. Jørgensen, T. Helgaker, G. E. Scuseria, and I. Schaefer, Henry F., J. Chem. Phys. **92**, 4924 (1990).
[81]O. Christiansen, H. Koch, and P. Jørgensen, J. Chem. Phys. **103**, 7429 (1995).
[82]H. Koch, O. Christiansen, P. Jørgensen, and J. Olsen, Chem. Phys. Lett. **244**, 75 (1995).
[83]J. Toulouse, F. m. c. Colonna, and A. Savin, Phys. Rev. A **70**, 062505 (2004).
[84]J. W. Knight, X. Wang, L. Gallandi, O. Dolgounitcheva, X. Ren, J. V. Ortiz, P. Rinke, T. Körzdörfer, and N. Marom, J. Chem. Theory Comput. **12**, 615 (2016).
[85]L. Gallandi, N. Marom, P. Rinke, and T. Körzdörfer, J. Chem. Theory Comput. **12**, 605 (2016), pMID: 26731340, https://doi.org/10.1021/acs.jctc.5b00873.
[86]M. J. Frisch, G. W. Trucks, H. B. Schlegel, G. E. Scuseria, M. A. Robb, J. R. Cheeseman, G. Scalmani, V. Barone, G. A. Petersson, H. Nakatsuji, X. Li, M. Caricato, A. V. Marenich, J. Bloino, B. G. Janesko, R. Gomperts, B. Mennucci, H. P. Hratchian, J. V. Ortiz, A. F. Izmaylov, J. L. Sonnenberg, D. Williams-Young, F. Ding, F. Lipparini, F. Egidi, J. Goings, B. Peng, A. Petrone, T. Henderson, D. Ranasinghe, V. G. Zakrzewski, J. Gao, N. Rega, G. Zheng, W. Liang, M. Hada, M. Ehara, K. Toyota, R. Fukuda, J. Hasegawa, M. Ishida, T. Nakajima, Y. Honda, O. Kitao, H. Nakai, T. Vreven, K. Throssell, J. A. Montgomery, Jr., J. E. Peralta, F. Ogliaro, M. J. Bearpark, J. J. Heyd, E. N. Brothers, K. N. Kudin, V. N. Staroverov, T. A. Keith, R. Kobayashi, J. Normand, K. Raghavachari, A. P. Rendell, J. C. Burant, S. S. Iyengar, J. Tomasi, M. Cossi, J. M. Millam, M. Klene, C. Adamo, R. Cammi, J. W. Ochterski, R. L. Martin, K. Morokuma, O. Farkas, J. B. Foresman, and D. J. Fox, "Gaussian~16 Revision A.03," (2019), gaussian Inc. Wallingford CT.
[87]I. Duchemin and X. Blase, J. Chem. Theory Comput. **16**, 1742 (2020).
[88]I. Duchemin and X. Blase, J. Chem. Theory Comput. **17**, 2383 (2021).
[89]X. Ren, P. Rinke, V. Blum, J. Wieferink, A. Tkatchenko, A. Sanfilippo, K. Reuter, and M. Scheffler, New J. Phys. **14**, 053020 (2012).
[90]F. Neese, F. Wennmohs, U. Becker, and C. Riplinger, J. Chem. Phys. **152**, 224108 (2020).
[91]P.-F. Loos, F. Lipparini, M. Boggio-Pasqua, A. Scemama, and D. Jacquemin, J. Chem. Theory Comput. **16**, 1711 (2020).
[92]P.-F. Loos, M. Comin, X. Blase, and D. Jacquemin, J. Chem. Theory Comput. **17**, 3666 (2021).
[93]"TURBOMOLE V7.5.1 2021, a development of University of Karlsruhe and Forschungszentrum Karlsruhe GmbH, 1989-2007, TURBOMOLE GmbH, since 2007; available from `https://www.turbomole.org`.".
[94]S. G. Balasubramani, G. P. Chen, S. Coriani, M. Diedenhofen, M. S. Frank, Y. J. Franzke, F. Furche, R. Grotjahn, M. E. Harding, C. Hättig, A. Hellweg, B. Helmich-Paris, C. Holzer, U. Huniar, M. Kaupp, A. Marefat Khah, S. Karbalaei Khani, T. Müller, F. Mack, B. D. Nguyen, S. M. Parker, E. Perlt, D. Rappoport, K. Reiter, S. Roy, M. Rückert, G. Schmitz, M. Sierka, E. Tapavicza, D. P. Tew, C. van Wüllen, V. K. Voora, F. Weigend, A. Wodyński, and J. M. Yu, J. Chem. Phys. **152**, 184107 (2020).
[95]Schrödinger, LLC, "The PyMOL molecular graphics system, version 2.5.2," (2021).
[96]S. R. Marder, C. B. Gorman, B. G. Tiemann, J. W. Perry, G. Bourhill, and K. Mansour, Science **261**, 186 (1993).
[97]A. Hellweg and D. Rappoport, Phys. Chem. Chem. Phys. **17**, 1010 (2015).
[98]J. Tomasi, B. Mennucci, and R. Cammi, Chem. Rev. **105**, 2999 (2005).
[99]J. Cerezo and F. Santoro, "Fcclasses 3.0 available from `http://www.pi.iccom.cnr.it/fcclasses`.".
[100]F. Santoro, R. Improta, A. Lami, J. Bloino, and V. Barone, J. Chem. Phys. **126**, 084509 (2007).
[101]A. Lami and F. Santoro, "Time-dependent approaches to calculation of steady-state vibronic spectra: From fully quantum to classical approaches," in *Computational Strategies for Spectroscopy* (John Wiley & Sons, Ltd, 2011) Chap. 10, pp. 475–516.
[102]J. Cerezo, J. Zúñiga, A. Requena, F. J. Ávila Ferrer, and F. Santoro, J. Chem. Theory Comput. **9**, 4947 (2013).
[103]E. Brémond, M. Savarese, C. Adamo, and D. Jacquemin, J. Chem. Theory Comput. **14**, 3715 (2018).
[104]C. Wang, W. Chi, Q. Qiao, D. Tan, Z. Xu, and X. Liu, Chem. Soc. Rev. **50**, 12656 (2021).
[105]B. Mennucci, A. Toniolo, and J. Tomasi, J. Am. Chem. Soc. **122**, 10621 (2000).
[106]I. Georgieva, A. J. A. Aquino, F. Plasser, N. Trendafilova, A. Köhn, and H. Lischka, J. Phys. Chem. A **119**, 6232 (2015).
[107]D. Jacquemin, E. A. Perpète, G. Scalmani, M. J. Frisch, R. Kobayashi, and C. Adamo, J. Chem. Phys. **126**, 144105 (2007).
[108]S. Grimme and F. Neese, J. Chem. Phys. **127**, 154116 (2007).
[109]B. I. Moore and J. Autschbach, J. Chem. Theory Comput. **9**, 4991 (2013).
[110]L. Goerigk, J. Moellmann, and S. Grimme, Phys. Chem. Chem. Phys. **11**, 4611 (2009).
[111]L. Goerigk and S. Grimme, J. Chem. Phys. **132**, 184103 (2010).
[112]D. Jacquemin, A. Planchat, C. Adamo, and B. Mennucci, J. Chem. Theory Comput. **8**, 2359 (2012).
[113]N. O. C. Winter, N. K. Graf, S. Leutwyler, and C. Hättig, Phys. Chem. Chem. Phys. **15**, 6623 (2013).
[114]F. J. Avila Ferrer and F. Santoro, Phys. Chem. Chem. Phys. **14**, 13549 (2012).
[115]F. J. Avila Ferrer, J. Cerezo, E. Stendardo, R. Improta, and F. Santoro, J. Chem. Theory Comput. **9**, 2072 (2013).
[116]A. Baiardi, J. Bloino, and V. Barone, J. Chem. Theory Comput. **9**, 4097 (2013).
[117]D. Barton, C. König, and J. Neugebauer, J. Chem. Phys. **141**, 164115 (2014).